Competing mechanisms on the strength of ion-irradiated Zr/Nb nanoscale multilayers: interface strength versus radiation hardening

M. Callisti[a,*], M. Karlik[b, c], T. Polcar[d, e]

[a] Department of Materials Science and Metallurgy, University of Cambridge, 27 Charles Babbage Road, Cambridge, CB3 0FS, United Kingdom

[b] Department of Materials, Faculty of Nuclear Sciences and Physical Engineering, Czech Technical University in Prague, Trojanova 13, 120 00 Prague 2, Czech Republic

[c] Department of Physics of Materials, Faculty of Mathematics and Physics, Charles University, Ke Karlovu 5, 121 16 Prague 2, Czech Republic

[d] National Centre for Advanced Tribology at Southampton, Faculty of Engineering and the Environment, University of Southampton, Southampton SO17 1BJ, UK

[e] Department of Control Engineering, Faculty of Electrical Engineering, Czech Technical University in Prague, Technicka 2, Prague 6, Czech Republic

*** Corresponding Author Information**
Dr. Mauro Callisti
mc2057@cam.ac.uk
Department of Materials Science and Metallurgy
Cambridge University, 27 Charles Babbage Road, Cambridge
CB3 0FS, United Kingdom
Office Phone: +44(0)1223 334434

Abstract

The structural stability and mechanical properties of sputter-deposited Zr/Nb nanoscale multilayers subjected to Si-ion irradiation were investigated in relation to the individual layer thickness. The interface density distribution played a major role on the nature and amount of accumulated radiation damage. The multilayer with a smaller periodicity experienced a significantly higher atomic-scale disorder and radiation hardening compared to the multilayer with thicker individual layers. In the latter case, an enhanced radiation damage tolerance was achieved due to the balance between competing deformation mechanisms.

Keywords: Radiation hardening, interfaces, multilayers, transmission electron microscopy (TEM), nanoindentation.

To guarantee longer and safer life cycles in new generation nuclear technologies, enhanced radiation damage tolerance is required for nuclear materials [1]. One of the main objectives in designing nuclear materials is to optimise structures able to sink radiation damage. Surfaces, grain boundaries and heterointerfaces revealed to be excellent sinks for radiation-induced point defects as they encourage vacancies-interstitial recombination [2], thus conferring to materials a self-healing character. With the aim of developing nanostructured materials with increasing radiation tolerance, sputter-deposited nanoscale metallic multilayers (NMMs) were often used as versatile model materials to design interfaces with various orientation relationships and properties [3, 4]. A large variety of interfaces was tested against extreme conditions with a particular focus on deformation mechanisms of He bubble-containing interfaces/materials [5-7]. It is generally accepted that radiation hardening due to He bubbles formation in the layers is drastically reduced or suppressed by increasing the interface density distribution in various interface systems (i.e. Cu/Nb [6-9], Cu/V [10, 11], Cu/Cu-Zr [12], V/Ag [13], Ag/Ni [14], etc.). Only a few number of studies was conducted to assess the structural evolution of interfaces subjected to heavy ion irradiation. Some of the most common heterointerfaces reported in the literature are: Cu/Fe [15], Cu/Nb [16], Cr/W [17], etc. Overall, it was observed that by increasing the interface density, a decreased amount of defects survived in the layers. However, there is a lack in the literature regarding the correlation between structural defects and deformation mechanisms in materials/interfaces irradiated with heavy ions. The mechanical behaviour of interfaces is a crucial aspect to be assessed as this significantly affects overall material properties. Recently, hcp-based NMMs started to attract some attention and cases of hcp-based NMMs are: Mg/Nb [18], Zr/Nb [19, 20], Co/Mo [21], Mg/Ti [22], Cu/Zr [23], etc.

Most of the studies on *hcp*-based NMMs focused on the structure-strength relationship of pristine NMMs, while no relevant investigations were performed to assess their behaviour after ion irradiation. To fill the gap, the Zr/Nb system, whose structure-strength relationship [19] and thermal stability [24, 25] are reported in detail in our previous studies, was used to investigate and correlate its structural and mechanical stability when subjected to irradiation by energetic particles.

Zr/Nb NMMs with two different periodicities L = 6 and 27 nm (hereinafter referred as Zr/Nb_6 and Zr/Nb_{27}) were deposited on Si substrates by magnetron sputtering as described elsewhere [19]. Zr/Nb_6 (total thickness of 1.48 μm) presented an individual layer thickness (h) of 3 nm ($h_{Zr} = h_{Nb}$), while for Zr/Nb_{27} (total thickness of 1.35 μm) h_{Zr} = 16 nm and h_{Nb} = 11 nm. The as-deposited multilayers were irradiated by Si^{1+} ions with an energy of 1.8 MeV and with two fluences (i.e. 4.0×10^{15} and 1.0×10^{16} ions/cm^2) which, according to SRIM [26] calculations, produced a peak damage of 5 and 13 dpa (hereinafter indicated as low and high dose), respectively at a depth of about 700-800 nm. Structural analyses on pristine and irradiated samples were performed by X-ray diffraction (XRD) and transmission electron microscopy (TEM). TEM/STEM observations and elemental analyses by EDX were carried out at 200 kV. Cross-sectional TEM samples were prepared by conventional methods. Mechanical properties of the multilayers were measured by nanoindentation according to the procedure outlined elsewhere [19].

Zr/Nb_{27} NMM presented parallel $(0002)_{Zr}$ and $(110)_{Nb}$ textures grown parallel to the substrate. Crystallographic analyses (XRD, SADPs) revealed formation of incoherent Zr/Nb interfaces. On the other hand, for Zr/Nb_6 beside a reduced grain size, a crystallographic reorientation for Zr (*hcp*) occurred, which led to a change in the orientation relationship between layers, i.e. (1010)Zr//(110)Nb, thus giving origin to semi-coherent Zr/Nb interfaces. Further details about

the structural and mechanical properties of the as-deposited multilayers are reported in our previous study [19].

After irradiation, XRD analyses revealed some changes for Zr/Nb6 associated with less prominent satellite peaks and a reduced FWHM for the main peak located at $2\theta \approx 35.6^{\circ}$ (Fig. 1a). The first aspect indicates a decreased level of interfacial coherency after irradiation. The second aspect is associated to a closer overlapping of the peaks originally associated to the Nb and Zr textures. This can be due to a closer match between the Zr and Nb lattice parameters or more likely to a partial amorphisation of one or both constituent layers. A much more complex pattern was observed for Zr/Nb_{27} after irradiation (Fig. 1b). The main textures were surrounded by symmetrically distributed secondary peaks (indexed as $\pm\, i$ in Fig. 1b). After a careful examination of the XRD patterns, it was concluded that no additional phases like silicides, due to Si ion implantation, formed in Zr/Nb27. These observations led us to attribute the presence of secondary (or satellite [27]) peaks to a radiation-induced transition of the Zr/Nb interfaces from incoherent to partially coherent. The other major change observed in Fig. 1b in relation to the radiation damage is a systematic and opposite shift of the (0002)Zr and (110)Nb peaks, which will be discussed later.

Finer structural analyses on NMMs irradiated with high dose were carried out by analytical S/TEM. Cross-sectional TEM samples for Zr/Nb_6 and Zr/Nb_{27} were first inspected across the entire films thickness to assess the elemental distribution after radiation experiments. HAADF-STEM images and EDX linescans revealed chemically sharp interfaces (see Fig. S1) and a homogeneous Si dispersion across the films thickness without any preferential segregation between Zr and Nb layers. Selected area electron diffraction patterns (SADPs) were acquired for the as-deposited and irradiated multilayers (Fig. 2). The as-deposited Zr/Nb_{27} presented a well-defined SADP with a six-fold symmetry and distinct $(0002)_{Zr}$ and $(110)_{Nb}$ textures (Fig. 2a). After irradiation, although the pattern still presented a six-fold symmetry (Fig. 2b), slightly

more continuous diffraction rings appeared. In addition, a closer overlapping of the main textures (highlighted in Fig. 2b) was also observed as anticipated by XRD analyses. Regarding the Zr/Nb_6, the major difference observed on the SADPs after irradiation is associated with the formation of more continuous diffraction rings (Fig. 2c-d), thus indicating either formation of smaller and randomly oriented crystallites or more likely a higher level of disorder in Zr and Nb layers.

Table 1 summarises the mechanical properties measured by nanoindentation on pristine and irradiated multilayers. Zr/Nb_{27} showed no appreciable changes in hardness and only a minor decrease in elastic modulus for an increasing level of damage. On the other hand, Zr/Nb_6 exhibited an appreciable hardening effect for higher doses, while only minor changes were found for the elastic modulus. In spite of the significant structural changes detected for Zr/Nb_{27} based on diffraction analyses, major variations in mechanical properties were only observed for Zr/Nb_6.

To gather a deeper understanding about the correlation between radiation-induced structural changes and corresponding mechanical properties, high-resolution TEM analyses were carried out on multilayers irradiated with high dose. After irradiation, the layered structure of Zr/Nb_{27} was retained (Fig. 3a). However, a careful examination of the atomic structure revealed structural changes at interfaces and in the grains interior of the constituent layers. Radiation-induced defects were in the form of disordered atomic domains resembling the result of collision cascades, as highlighted in Fig. 3c. Nano-voids were also occasionally observed as illustrated in Fig. 3d, where the inset shows some very small voids consisting of a few vacant atomic sites. As anticipated by XRD, an enhanced degree of coherency was observed for the Zr/Nb interfaces (Fig. 3b) across the film thickness and regardless of the layers stacking sequence. This transition was driven by the development of internal stresses associated with radiation damage. Specifically, due to the constraining effect of adjacent layers, formation of

atomic-scale disorder in the grains interior resulted in the development of compressive stresses especially in Nb layers (see Fig. 1b). Stress was partially released through formation of twins parallel to the interfaces in Zr layers (Fig. 3b) and bending of the Nb atomic planes close to interfaces (see Fig. S2), thus encouraging formation of more coherent Zr/Nb interfaces.

A much more complex scenario at the atomic scale was found for the irradiated Zr/Nb_6 (Fig. 4). Although the layered structure was mostly retained, severely disrupted crystallites were observed and a disordered structure formed in the layers as documented by the almost continuous diffraction rings in the inset of Fig. 4a. The atomic arrangement inside the layers was not always obvious (Fig. 4b) and often interfaces could not be identified unambiguously.

In what follows, we correlate the observed structural changes with the resulting mechanical properties of the multilayers by quantifying the interaction of activated dislocations with interfaces and radiation-induced defects.

For the as-deposited Zr/Nb_6, a modified interface barrier strength (IBS) model was proposed to calculate the flow strength [19], which amounted to 1.85 GPa ($\sigma=H/\alpha$, with a Tabor factor α of 2.7). However, for the irradiated Zr/Nb_6, due to its highly disordered structure, the IBS model resulted inadequate. By using the rule-of-mixture (ROM) to combine the flow strength of crystalline Zr and Nb monolithic layers (1.6 and 1.25 GPa [28], respectively) a strength of about 1.4 GPa was calculated. The yield strength ($\sigma=H/2.7$) for irradiated Zr/Nb_6 multilayers was of 2.1 and 2.3 GPa for low and high dose, respectively. Therefore, the ROM largely underestimates the strength of the irradiated Zr/Nb_6. This difference is associated with the fact that although the layers are still mostly crystalline, the high density of radiation-induced defects in the grains along with less coherent interfaces formed strong barriers against dislocations movement, thus causing a significant strengthening effect.

For the as-deposited Zr/Nb_{27}, the flow strength, well-described by the confined layer slip (CLS) model [19], amounted to 1.93 GPa. After irradiation, due to formation of more coherent

interfaces and of internal defects, different mechanisms were considered to quantify the flow strength. In this case, the IBS model (Eq. 1-3 [29, 30]) was used to account for the strength of radiation-induced (partially) coherent interfaces against dislocations transmission.

$$\tau_{image} = \frac{\mu_{Nb}-\mu_{Zr}}{\mu_{Nb}+\mu_{Zr}} \frac{\mu_{Zr}\, sin\, \varphi}{8\pi} \quad (1)$$

$$\tau_{misfit} = \alpha\mu^{*}\left(\xi - \frac{b}{2h}\right) \quad (2)$$

$$\sigma_{IBS} = M(\tau_{image} + \tau_{misft}) \quad (3)$$

By using the shear moduli μ_{Zr} = 33 GPa and μ_{Nb} = 37.5 GPa, a Saada's constant α = 0.5, a misfit strain ξ = *b/s* (where b is the Burgers vector and *s* is the distance between interfacial misfit dislocations found to be in a range of 7–12 nm from HR-TEM images), an effective shear modulus μ^{*} = 35.1 GPa, *b* = 0.3232 nm, a Taylor factor *M* = 3.1 and a layer thickness $h = h_{Zr}$ (Zr layers control the deformation mechanism in Zr/Nb_{27} [19]), a σ_{IBS} in a range of 1.4 – 2.2 GPa was calculated. The other component to be considered is the strength originating from the interaction between activated dislocations and radiation-induced defects in the grains interior. For this, we used the general theory of obstacles strengthening [31]. By assuming a strong interaction between dislocations and localised defects, the flow stress can be calculated by Eq. 4 [29].

$$\tau_{s.o} \simeq 0.84 \frac{\mu\, b}{\Lambda} (cos\phi_c)^{3/2} \quad (4)$$

Where ϕ_c is the critical angle that a dislocation line forms with respect to the direction of the resistant force exerted by the obstacle. ϕ_c can be assumed to be ≈ 0 for random arrays of strong obstacles. For Zr/Nb_{27} irradiated with high dose, the average spacing (Λ) between defects contained in the same layer was measured on the HR-TEM images across the film thickness. An average distance of 8.7±3.5 nm (~h_{Zr}/2) was obtained between defects formed in the Zr layers, which were considered as localised strong obstacles. Therefore, by using the values for μ, *b* and Λ reported above, a flow strength for strong obstacles ($\tau_{s.o}$) ranging between 0.7–1.7

GPa is calculated, which corresponds to a normal flow stress $\sigma_{s.o}$ ranging between 2.2–5.3 GPa. It is reasonable to consider as a more representative $\sigma_{s.o}$ the lower bound (2.2 GPa), as dislocations tend to propagate primarily through energetically less demanding paths. A comparison of the normal flow strength estimated from nanoindentation data (1.9 GPa) against those calculated by the IBS model (1.8 GPa) and based on the obstacles strengthening theory (2.2 GPa) suggests that both deformation mechanisms affect the strength of the irradiated Zr/Nb_{27}. The minor variation in mechanical properties (Tab. 1) found for Zr/Nb_{27} in as-deposited and irradiated conditions is attributed to a balance between these competing mechanisms. On one side, formation of more coherent Zr/Nb interfaces facilitates dislocations transmission, thus causing a softening effect compared to the originally incoherent Zr/Nb interfaces. On the other hand, formation of obstacles in the grain interiors obstructs dislocations movement, thus causing an opposite effect (hardening). It is concluded that the multilayer with the larger periodicity is more radiation damage tolerant compared to the finer layered structure. In summary, we examined the effects of radiation damage on the structural and mechanical properties of Zr/Nb NMMs with different periodicities. For the multilayer with a periodicity of 6 nm, Si-ion irradiation led to a considerable level of atomic-scale disorder, thus causing a significant radiation hardening. For the multilayer with a periodicity of 27 nm, radiation damage was in the form of disordered (amorphous-like) domains and occasionally nano-voids. In addition, an increasing degree of interfacial coherency between layers was observed in relation to the radiation dose. In spite of the observed damage, no appreciable hardening effects were found in the latter case. This enhanced radiation damage tolerance resulted from the balance between two competing deformation mechanisms, mainly dislocation transmission across radiation-induced (partially) coherent interfaces and dislocation interaction with radiation-induced defects in the grains interior.

Acknowledgment

M.C. acknowledges Innovate UK (reference number: 113072) for financial support. This study was also supported by the Czech Science Foundation through the project 17-17921S and by the ERDF project No. CZ.02.1.01/0.0/0.0/15_003/0000485. Dr Vladimir Havranek, NPI CAS Rez (Czech Republic), is acknowledged for irradiation experiments, which were carried out at the CANAM (Centre of Accelerators and Nuclear Analytical Methods) infrastructure LM 2015056, supported by OP RDE, MEYS, Czech Republic under the project CANAM OP, CZ.02.1.01/0.0/0.0/16_013/0001812. Part of the data published in this paper is available from the University of Cambridge repository at https://doi.org/10.17863/CAM.21566.

References

[1] P. Hosemann, D. Frazer, M. Fratoni, A. Bolind, M.F. Ashby, Scripta Mater. 143 (2018) 181-187.

[2] X.-M. Bai, A.F. Voter, R.G. Hoagland, M. Nastasi, B.P. Uberuaga, Science 327 (2010).

[3] A. Misra, M.J. Demkowicz, X. Zhang and R.G. Hoagland, JOM, 59, 62 (2007).

[4] Mikhail Zhernenkov, Simerjeet Gill, Vesna Stanic, Elaine Di Masi, Kim Kisslinger, J. Kevin Baldwin, Amit Misra, M. J. Demkowicz, Lynne Ecker, Appl. Phys. Lett. 104, 241906 (2014).

[5] M. Callisti, M. Karlik, T. Polcar, J. Nucl. Mater. 473 (2016) 18-27.

[6] N. Li, N.A. Mara, Y.Q. Wang, M. Nastasi, A. Misra, Scripta Mater. 64 (2011) 974-977.

[7] M.J. Demkowicz, L. Thilly, Acta Mater. 59 (2011) 7744-7756.

[8] K. Hattar, M.J. Demkowicz, A. Misra, I.M. Robertson, R.G. Hoagland, Scripta Mater. 58 (2008) 541-544.

[9] N. Li, M. Nastasi, A. Misra, Int. J. Plast. 32-33 (2012) 1-16.

[10] E.G. Fu, J. Carter, G. Swadener, A. Misra, L. Shao, H. Wang, X. Zhang, J. Nucl. Mater. 685 (2009) 629-632.

[11] E.G. Fu, A. Misra, H. Wang, Lin Shao, X. Zhang, J. Nucl. Mater. 407 (2010) 178-188.

[12] J.Y. Zhang, Y.Q. Wang, X.Q. Liang, F.L. Zeng, G. Liu, J. Sun, Acta Mater. 92 (2015) 140-151.

[13] Q.M. Wei, N. Li, N. Mara, M. Nastasi, A. Misra, Acta Mater. 59 (2011) 6331-6340.

[14] K.Y. Yu, Y. Liu, E.G. Fu, Y.Q. Wang, M.T. Myers, H. Wang, L. Shao, X. Zhang, J. Nucl. Mater. 440 (2013) 310-318.

[15] Y. Chen, N. Li, D.C. Bufford, J. Li, K. Hattar, H. Wang, X. Zhang, J. Nucl. Mater. 475 (2016) 274-279.

[16] Shimin Mao, Sezer Ozerinc, William P. King, Robert S. Averbacka, Shen J. Dillon, Scripta Mater. 90-91 (2014) 29-32.

[17] Feida Chen, Xiaobin Tanga, Hai Huang, Jian Liu, Huan Li, Yunlong Qiu, Da Chen, Appl. Surf. Scie. 357 (2015) 1225-1230.

[18] B. Ham, X. Zhang, Mater. Sci. Eng. A 528 (2011) 2028-2033.

[19] M. Callisti, T. Polcar, Acta Mater. 124 (2017) 247-260.

[20] M.A. Monclús, M. Callisti, T. Polcar, L.W. Yang, J. Llorca, J.M. Molina-Aldareguía, Acta Mater. 122 (2017) 1-10.

[21] G.H. Yang, B. Zhao, Y. Gao, F. Pan, Surf. Coat. Technol. 191 (2005) 127-133.

[22] Y.Y. Lu, R. Kotoka, J.P. Ligda, B.B. Cao, S.N. Yarmolenko, B.E. Schuster, Q. Wei, Acta Mater. 63 (2014) 216-231.

[23] J.Y. Zhang, S. Lei, Y. Liu, J.J. Niu, Y. Chen, G. Liu, X. Zhang, J. Sun, Acta Mater. 60 (2012) 1610-1622.

[24] M.A. Monclús, M. Callisti, T. Polcar, L.W. Yang, J. Llorca, J.M. Molina-Aldareguía, Acta Mater. 122 (2017) 1-10.

[25] M.A. Monclús, M. Callisti, T. Polcar, L.W. Yang, J.M. Molina-Aldareguía, J. Llorca, J. Mater. Sci. (2018) 53:5860-5878.

[26] J. Ziegler, The Stopping and Range of Ions in Matter (SRIM), 2011. http://www.srim.org.

[27] B.M. Clemens, J.G. Gay, Phys. Rev. B 35 (17) (1987) 9337-9340.

[28] J.Y. Zhang, X. Zhang, R.H. Wang, S.Y. Lei, P. Zhang, J.J. Niu, G. Liu, G.J. Zhang, J. Sun, Acta Mater. 59 (2011) 7368e7379.

[29] Koehler JS. Phys. Rev. B 1970, 2:547.

[30] Rao SI, Hazzledine PM. Philos. Mag. A 2000, 80:2011.

[31] D. Hull, D. J. Bacon, Introduction to dislocations, fifth ed., Butterworth-Heinemann 2011.

Figures caption

Fig. 1. XRD analysis of the as-deposited and irradiated multilayers with low and high dose: (a) Zr/Nb_{27} and (b) Zr/Nb_6. Dashed lines indicate peak position changes as a function of the radiation damage.

Fig. 2. Selected area electron diffraction patterns (SADPs) acquired over the entire film cross-section for as-deposited and irradiated (with high dose, H-D) Zr/Nb_{27} (a)-(b) and Zr/Nb_6 (c)-(d) multilayers. The arrow in each figure indicates the film growth direction, while the dashed circles in (b) highlight the $(0002)_{Zr}$ and $(110)_{Nb}$ textures.

Fig. 3. Cross-sectional high-resolution TEM images of the Zr/Nb_{27} irradiated with high dose. (a) Layered structure. (b) Partially coherent interfaces in the region highlighted by the window in (a); the arrow highlights a twin formed parallel to the interface. (c) Typical atomic-scale

disorder observed in the Zr layers. (d) Atomic-scale disorder and voids observed in the Nb layer; the inset shows disruptions of the atomic structure close to the interface (Zr on the left).

Fig. 4. Cross-sectional high-resolution TEM images of the Zr/Nb6 irradiated with high dose: (a) layered structure and corresponding diffraction (FFT) pattern in the inset, (b) magnified region showing the typical atomic disorder inside Zr and Nb layers.

Tables caption

Tab. 1. Mechanical properties measured by nanoindentation on the as-deposited and irradiated Zr/Nb multilayers. The elastic modulus (E) of the multilayers was calculated from the reduced elastic modulus by using a Poisson's ratio and elastic modulus for the diamond tip of 0.07 and 1141 GPa, respectively. An average Poisson's ratio for the NMMs was calculated by using $\nu_{Zr} = 0.34$ and $\nu_{Nb} = 0.4$.

Figures

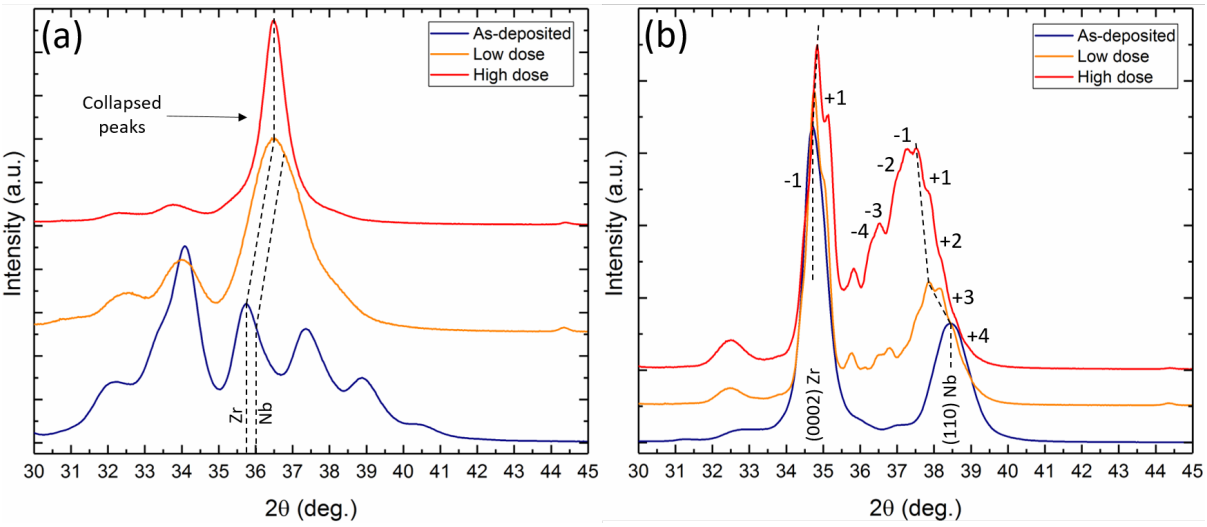

Fig. 1

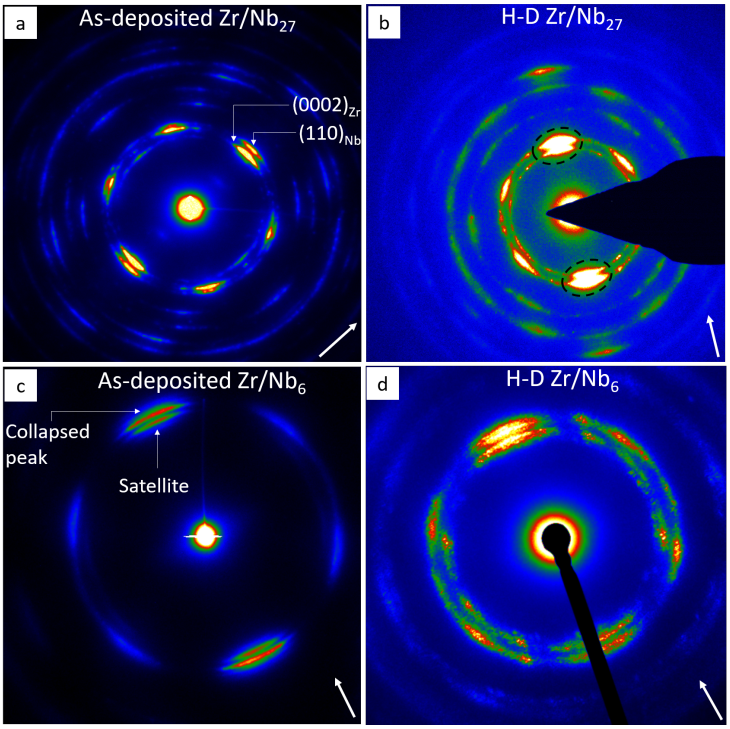
a
As-deposited Zr/Nb27
(0002)Zr
(110)Nb
b
H-D Zr/Nb27
c
As-deposited Zr/Nb6
Collapsed peak
Satellite
d
H-D Zr/Nb6

Fig. 2

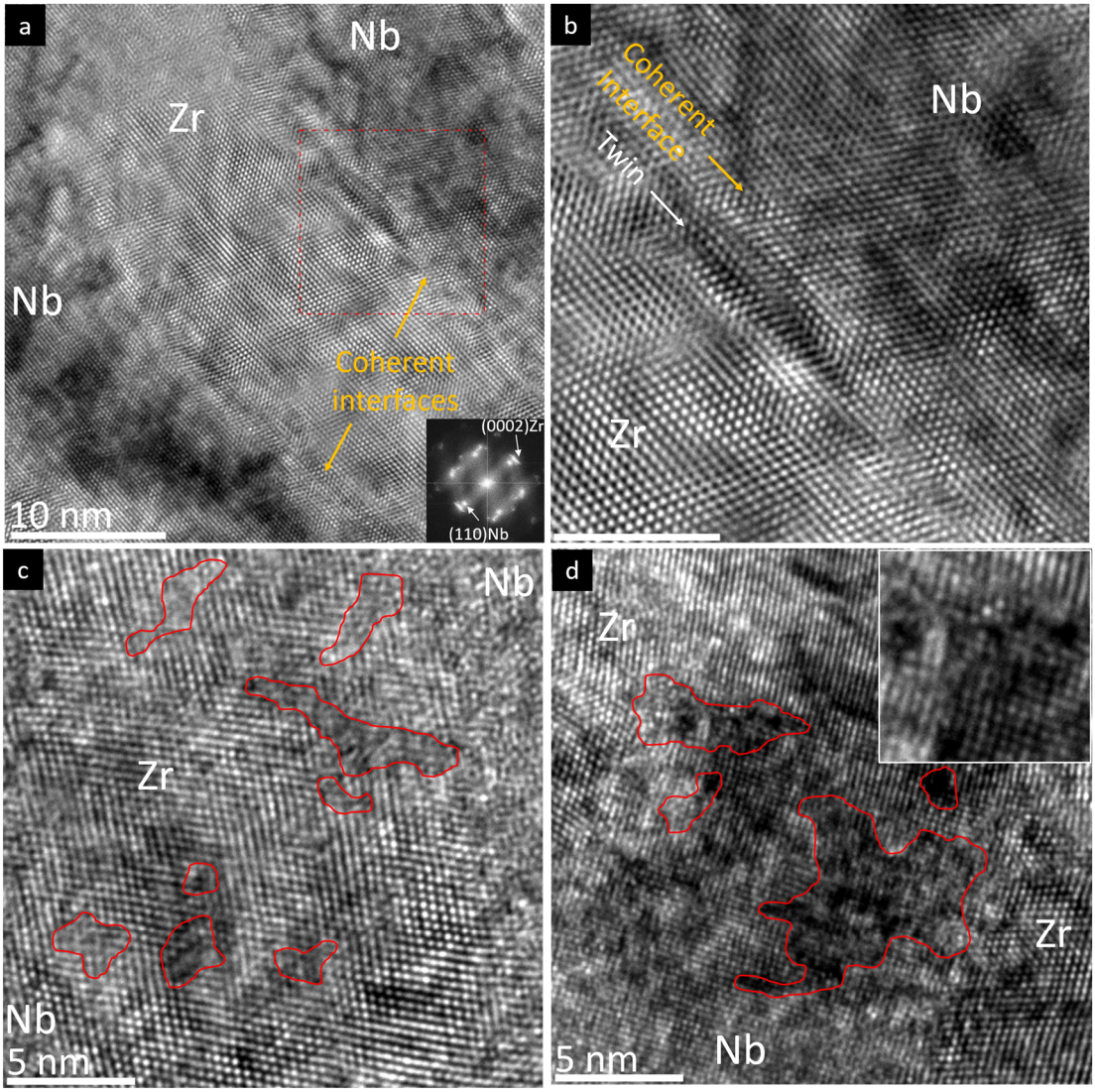
a
Nb
Zr
Nb
Coherent
interfaces
(0002)Zr
(110)Nb
10 nm
b
Coherent
Interface
Twin
Nb
Zr
c
Nb
Zr
Nb
5 nm
d
Zr
Zr
5 nm
Nb

Fig. 3

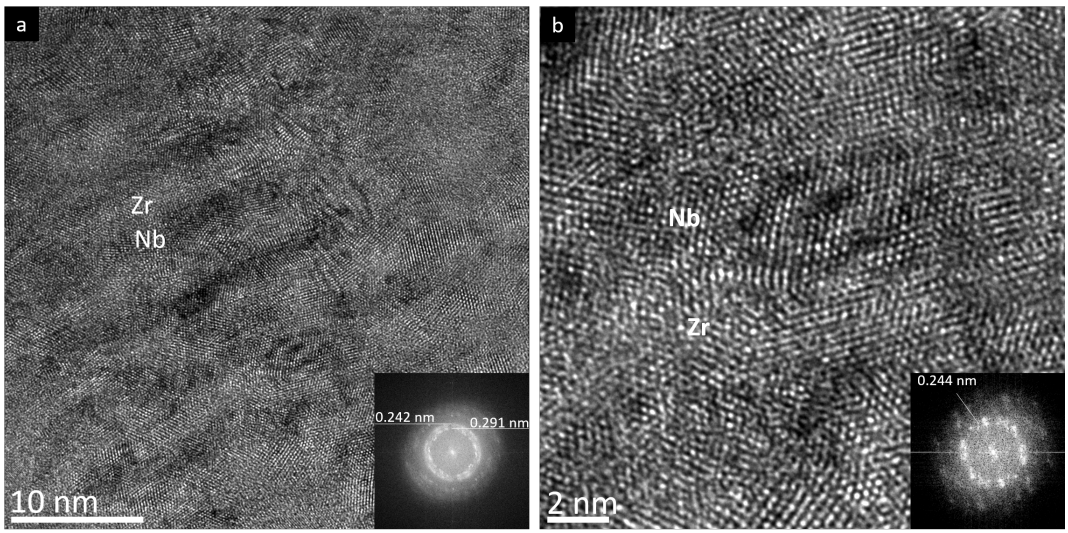
a
Zr
Nb
0.242 nm
0.291 nm
10 nm
b
Nb
Zr
0.244 nm
2 nm

Fig. 4

Tables

Tab. 1

	Pristine		Low Dose		High Dose	
	Zr/Nb_6	Zr/Nb_{27}	Zr/Nb_6	Zr/Nb_{27}	Zr/Nb_6	Zr/Nb_{27}
Hardness (GPa)	5 ± 0.3	5.2 ± 0.2	5.7 ± 0.5	5.2 ± 0.3	6.2 ± 0.5	5.1 ± 0.2
Elastic Modulus (GPa)	119.3 ± 5	136.5 ± 5	116.1 ± 5	126.6 ± 6	115.6 ± 4	122.4 ± 5

Graphical abstract